



# Effect of Reflux Hole on the Transient Flow Characteristics of the Self-Priming Sewage Centrifugal Pump

P. Zhou<sup>†</sup>, Z. Wu, J. Mou, D. Wu, S. Zheng and Y. Gu

*College of Mechanical Engineering, Zhejiang University of Technology, Hangzhou, Zhejiang, 310014, China*

<sup>†</sup>*Corresponding Author Email: peijianzhou@gmail.com*

(Received May 18, 2018; accepted December 1, 2018)

## ABSTRACT

The reflux hole has a large effect on the performance of self-priming centrifugal pumps. In order to study the effects of the reflux hole on the performance and transient flow characteristics of the self-priming centrifugal pump, four different areas of the reflux hole inside an external mixed self-priming pump were proposed. The 3D transient flow was numerically simulated under different operating conditions for the investigated pump. The differential pressure, reflux quantity and transient flow characteristics near the reflux hole were analysed, and then the effects of the reflux hole area on the pressure fluctuation characteristics and performance of the pump were further researched. The results show that the differential pressure and reflux quantity is zero around the best-efficiency point. The vorticity magnitude near the exit of the reflux hole is significant, and the unsymmetrical flow structures represent periodic motion over time in the cross-section. The pressure fluctuation intensities of monitoring points P<sub>2</sub>-P<sub>5</sub> upstream of the reflux hole were generally larger than others and decreased with a decrease in reflux hole area. With a decrease of the reflux hole area, the performance of the pump improved to some extent.

**Keywords:** Centrifugal pump; Reflux hole; Transient flow characteristics; Pressure fluctuation.

## NOMENCLATURE

$A_K$	reflux hole area	$\Delta p$	difference between instantaneous static pressure and mean pressure
$b_2$	impeller outlet width	$Q$	flow rate
$C_p$	pressure fluctuation coefficient	$Q_d$	design flow rate
$D_2$	impeller outlet diameter	$Q_r$	reflux flow rate
$D_i$	impeller suction diameter	$T$	passing period of blade
$d_K$	equivalent diameter	$\Delta t$	time-step size
$H$	head	$u_2$	circumferential velocity at impeller outlet
$H_d$	design head		
$K_{AK}$	experience factor	$\eta$	efficiency
$n$	rotational speed	$\rho$	water density

## 1. INTRODUCTION

Self-priming pumps, as a type of centrifugal pump, are widely used in agricultural irrigation, municipal sewage, petrochemical metallurgy, the chemical industry, etc. for their good self-priming performance. Compared with ordinary centrifugal pumps, self-priming pumps have some special structures, such as a gas-liquid separation chamber, a reflux hole, etc. The reflux hole is located between the volute and the gas-liquid separation chamber. When a self-priming pump

starts working, the air in suction line is encouraged to mix with the initial liquid at the outer edge of the impeller, and the mixture is conveyed through the volute to the gas-liquid separation chamber within the pump casing where the effective separation of air and liquid takes place. And the air free liquid is recycled back to the impeller through the reflux hole in the wall of the volute. The self-priming pump uses an initial quantity of liquid to create a partial vacuum as it removes air from the suction line. The vacuum causes atmospheric pressure to push fluid to the pump

through the suction line, until all the air has been evacuated from the suction line. At which point the pump will commence to discharge. (Lv, 2005; Shepard, 2013). Under the premise that the pump can achieve self-priming function, when the reflux hole area is large, a large amount of liquid flow back into the volute through the reflux hole, although the self-priming time is short, the suction lift is low, and the efficiency and the head are also decreased. Conversely, when the self-priming time is long, the suction lift is high. Obviously, the reflux hole is one of the most important factors affecting the self-priming and hydraulic performance of the self-priming centrifugal pump. However, during the normal operation of the self-priming pump, the reflux hole will lead to increased volume loss in the pump, decreasing the efficiency (Guan, 2011; Li, 2010; Yuan, 2015). Otherwise, due to the comprehensive effect of the reflux hole and the rotor-stator interaction, the flow field inside the volute is more complex.

A great deal of research has been done into the self-priming characteristic. As early as 1949, Hermann (1949) provided a useful reference value for the design of a self-priming centrifugal pump. Furthermore, the self-priming performance of the twisted-blade pump was studied by Hubbard (2000). In 2004, a comprehensive analysis and study of the self-priming centrifugal pump was carried out by Kanute (2004), from the working principle to the design method. Regarding the reflux hole in the self-priming pump, the effect of reflux hole on the self-priming performance was studied by Li (1982) and the design of the elastic value was carried out. Yi (1991) and Chen (1998; 1990) undertook many experimental studies on the self-priming centrifugal pump, including on the design method, factors influencing the self-priming performance, the effect of the reflux hole on self-priming performance curves, the correlations among reflux hole area, self-priming time and suction lift and the empirical equation for the reflux hole critical area. Wang (2017) studied the effects of impeller trim on performance of two-stage self-priming centrifugal pump.

Nowadays, numerical simulation technology has become a well-researched area in the study of the centrifugal pump. However, at present, the research is mainly focused on the unsteady flow dynamic characteristics of ordinary centrifugal pumps. Tan (2015) investigated unsteady flows in a centrifugal pump volute under non-cavitation and cavitation conditions using a computational fluid dynamics framework combining the re-normalization group  $k-\epsilon$  turbulence model and the mass transport cavitation model. Shi (2014) simulated the unsteady flow for non-cavitation and cavitation inside different centrifugal pumps and analysed the flow characteristics for non-cavitation and cavitation. The results show that the maximum pressure fluctuation is caused by the strong secondary flow vortex in the volute cross-section. Regarding the numerical simulation of the self-priming pump, most of the researches focuses on the numerical simulation analysis of the gas-liquid two-phase flow during the self-priming process. (Huang, 2014; Li, 2015; Li, 2013; Liu, 2009; Wang, 2009).

In conclusion, the reflux hole is an important factor that affects the self-priming performance and the energy performance of the self-priming centrifugal pump. However, there are no particular studies in the literature on the effect of the reflux hole on the volute pressure fluctuation characteristics and energy performance, or the transient flow characteristics near the reflux hole in the volute. In this paper, an external mixed self-priming pump with different reflux hole areas was chosen as the research object. The three-dimensional unsteady flows under various operating conditions of the investigated pump were numerically simulated, transient flow characteristics near the reflux hole were analysed and the effects of reflux hole area on the pressure fluctuation characteristics and energy performance of the pump were investigated, to provide a reference for the optimization of the hydraulic performance of the self-priming pump.

## 2. COMPUTATIONAL MODEL AND NUMERICAL METHOD

### 2.1 Parameters of Model

A self-priming centrifugal pump, with a maximum suction lift of 7 m, was selected as the research object. Its basic parameters are shown in Table 1. The reflux hole area is 400 mm<sup>2</sup>, and the angle between the reflux hole position to the tongue is 202°. These values are in the design requirement range (Sha, 1999). A cross-sectional view of the 3D view of the pump is shown in Fig. 1.

**Table 1 Main design parameters of the investigated pump**

Parameters	Values
$Q_d$ (design flow rate, m <sup>3</sup> /h)	65
$H_d$ (design head, m)	40
$n$ (rotational speed, rpm)	2,900
$D_i$ (impeller suction diameter, mm)	84
$D_2$ (impeller outlet diameter, mm)	190
$b_2$ (impeller outlet width, mm)	38

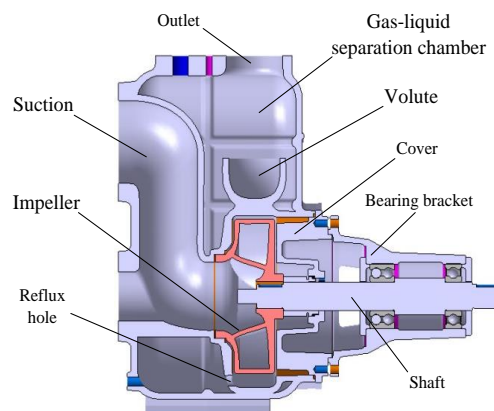


**Fig. 1. Cross-sectional view of the 3D pump.**

The optimum reflux hole area should cause the minimum hydraulic loss, on the assumption that it

meets the self-priming performance criteria. According to the traditional empirical formula, Eqs. (1) - (2) (Sha, 1999), the reflux hole area is 266 mm<sup>2</sup> - 598 mm<sup>2</sup>.

$$d_K = K_{AE} \sqrt[3]{Q/n} \quad (1)$$

$$A_K = \pi d_K^2 / 4 \quad (2)$$

where  $A_K$  is the reflux hole area,  $d_K$  is the equivalent diameter and  $K_{AK}$  is the experience factor with a value range from 1 to 1.5.

Therefore, the reflux hole area of the investigated pump should be further optimized. Four schemes for the reflux hole area were proposed: scheme 1 (400 mm<sup>2</sup>), scheme 2 (330 mm<sup>2</sup>), scheme 3 (260 mm<sup>2</sup>) and scheme 4 (no reflux hole). Numerical simulations were conducted for a range of flow rates ( $0.4Q_d - 1.4Q_d$ ). Then the effects of different reflux hole areas on the internal flow characteristics and the hydraulic performance were compared and analysed.

### 2.2 3D Modeling and Mesh

For the numerical simulation, the computational domain includes the investigated pump inlet pipe, outlet pipe, suction chamber, gas-liquid separation chamber, impeller, and volute with reflux hole. Due to the complexity of the computational domain, a 3D unstructured tetrahedral mixed mesh was used. Taking into account the quality of the grid and the accuracy of the calculation, and in order to control the maximum size of the grid cell in the fluid field of the impeller and volute, the key parts such as reflux hole, vanes and tongue, are encrypted locally. In order to eliminate the influence of the number of grids on the calculated results, the grid independence is analysed. Grid numbers of 1.35 million, 1.92 million and 3.23 million were used for the numerical simulation and the calculated head was 38.21 m, 38.84 m and 38.86 m respectively. Considering the accuracy and efficiency determination, 1.92 million is the most reasonable number. The outcome of the grid independence analysis is shown in Fig. 2. The  $y^+$  of each part is between 30 and 200, which meets the requirements of the standard wall function. Figure 3 shows the computational domain and mesh of the self-priming pump.

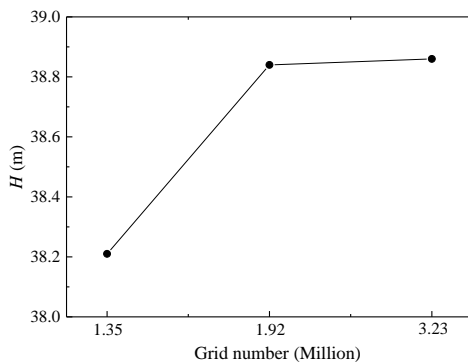


Fig. 2. The outcome of the grid independence analysis.

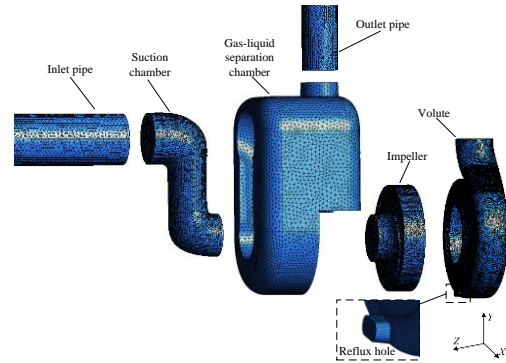


Fig. 3. Computational domain and mesh of the self-priming pump.

### 2.3 Calculation Methods and Monitoring Points

The numerical simulation is implemented using a commercial code (FLUENT). The finite volume method was adopted as a discrete method for the control equations (Reynolds-averaged Navier-Stokes equations). Referring to the commonly used turbulence model for centrifugal pump numerical calculations (Derakhshan, 2008; González, 2002), standard  $k-\epsilon$  turbulence model was used in the numerical simulation, which is a time-honored model for engineering applications. The pressure-velocity coupling was calculated using the SIMPLEC algorithm. The momentum, turbulence kinetic energy and dissipation rate equations were dispersed by second-order upwind (González, 2002; Wu, 2014). The inlet velocity- was imposed at the inlet and the outflow boundary condition was given at the outlet. No slip conditions were used at the wall. The roughness height was set at 0.02 mm and the roughness constant was set at 0.5 for all the computational domains except the inlet and outlet pipes. The steady calculation results were used as an initial value for the unsteady calculation. A total of 30 time steps are usually set per impeller revolution in the unsteady calculation for a multi-vane pump (Shi, 2014). Considering the wider impeller flow channel of a double-vane pump, 60 time steps per impeller revolution were set in this study. The time-step size is  $\Delta t=0.0001.724$  s.

As shown in Fig. 4, pressure monitoring points  $P_1 - P_8$  are located in the near-wall region to record the pressure fluctuation.  $P_1$  is at the tongue tip, and  $P_2$  to  $P_8$  are distributed around the circumference every 45°. Figure 4(b) shows that there are two monitoring planes at each side of the reflux hole.

### 2.4 Experiment Verification

A hydraulic facility designed according to International Standards (ISO 9906:2012) is used for the experiment. The experimental bench for the self-priming centrifugal pump is shown in Fig. 5. In order to measure the self-priming time of the self-priming centrifugal pump, the pump is placed on a platform. The distance between inlet and liquid level (suction lift) is 4 m, as shown in Fig. 5. With the power supply, the motor drives the impeller to rotate at a rated speed. A FAST Technologies torque meter was available for the experiment. The

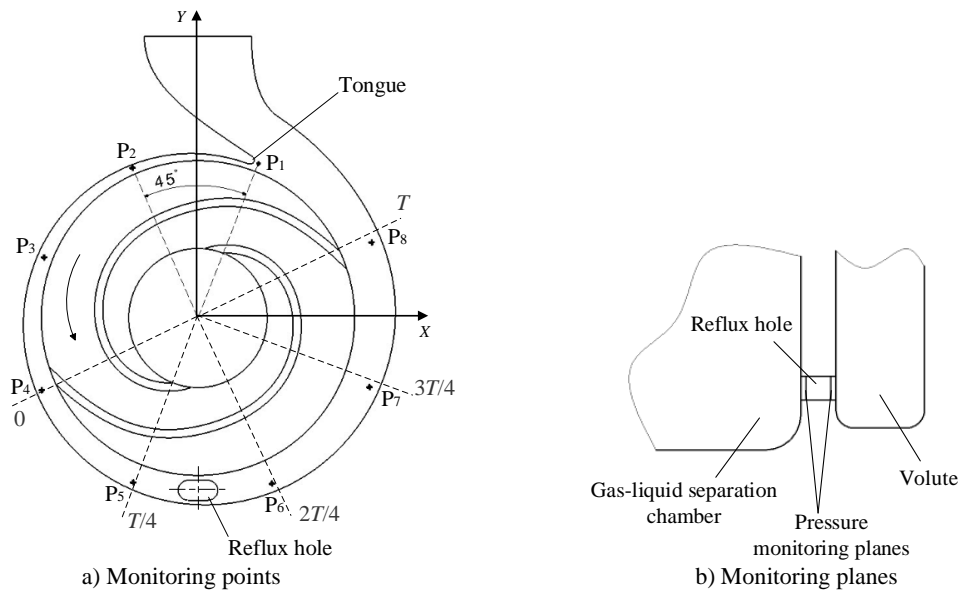
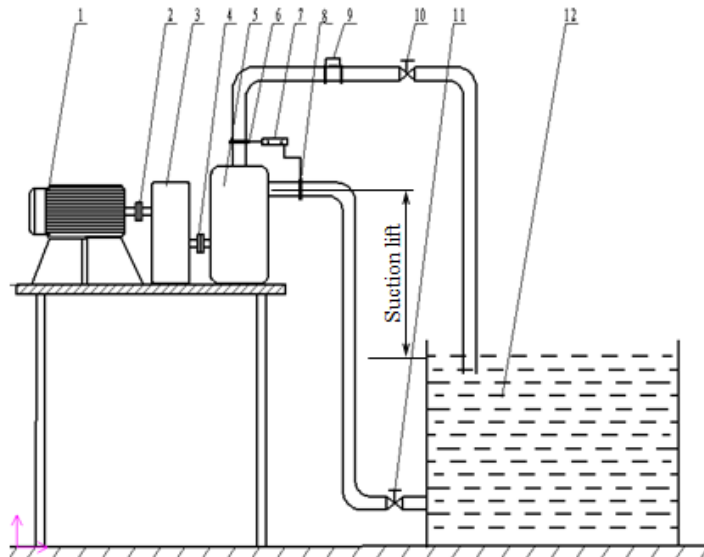


**Fig. 4. Locations of pressure monitoring points and planes.**



1 – electric motor; 2 – coupler; 3 – speed-changing case; 4 – coupler; 5 – pump; 6 – pressure sensor in the outlet; 7 – pressure display; 8 – pressure sensor in the inlet; 9 – electromagnetic flowmeter; 10 – sluice valve; 11 – sluice valve; 12 – water tank.

**Fig. 5. Sketch of self-priming test bench.**

torque range is 0-175 N•m and the combined uncertainty of this torque meter and the amplification system was kept under  $\pm 0.2\%$  for the particular values of the experiments.

The time period is recorded from when the power is turned on to when the centrifugal pump completes the self-priming process. The experiment shows that the self-priming time is 122 s with 4 m of suction lift. The flow rate uncertainties are calculated and found to be always less than 2.5%. Both the head and the efficiency uncertainties are kept below 3%, within the same confidence level. The resulting head and efficiency, as well as the signals from the tachometer are digitized and stored in a personal

computer equipped with a multichannel analogue-to-digital conversion card.

In order to verify the accuracy of the simulation results, the results of the investigated pump (scheme 1) were compared with the experimental results. The performance curves are shown in Fig. 6. As shown in Fig. 6, the head ( $H$ ) and efficiency ( $\eta$ ) of the simulation are slightly higher than the experimental values, which is due to the fact that the impeller inlet ring is simplified, and the volume loss of the seal gap is not taken into consideration. However, the largest deviation under various flow rates is less than 5%. This indicates agreement between the simulation and experiment.

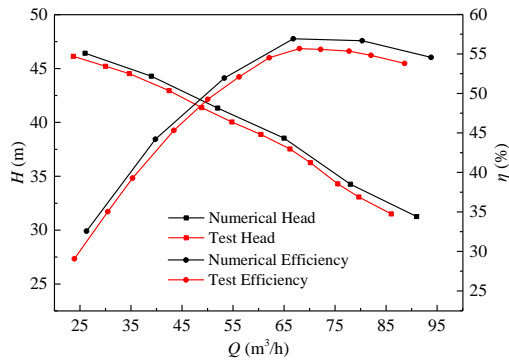


**Fig. 6. Comparison of performance curves between calculation and experiment.**

### 3. INFLUENCE OF DIFFERENT CONDITIONS ON FLOW STATE

Various 3D streamlines inside the pump for scheme 1 are shown in Fig. 7. The fluid flows into the pump from the inlet, passes by the suction chamber and flows into the impeller. Then, it is forced into the volute casing by the high-speed rotation of the impeller, flows into the gas-liquid chamber through the outlet of the volute casing and is finally discharged from the pump outlet. As shown in Fig. 7(a), at a low flow rate ( $0.4Q_d$ ), the streamlines in the separation chamber are more chaotic. The flow at the left side of the volute exit, especially, is quite disordered. It can be clearly seen that some of the fluid flows into the volute through the reflux hole, then flows into the separation chamber again with the liquid rotating at high speed, driven by the impeller. It can be seen that only a small part of the fluid is discharged from the pump outlet. The rest flows into the separation chamber again to form an annular flow, thereby increasing the volume loss. As shown in Fig. 7(b), under the design flow rate ( $1.0Q_d$ ), annular flow also occurs in the separation chamber but is relatively stable. At a high flow rate ( $1.4Q_d$ ), as seen in Fig. 7(c), the streamlines at the reflux hole show another flow state. The fluid in the separation chamber cannot flow into the volute casing but is blocked in the reflux hole and flows back into the separation chamber. The reason is that the pressure in the volute casing increases at large flow rates, so it can hold back the reflux flow. The blocked fluid reverses into the separation chamber.

Figure 8 illustrates the static pressure distribution and streamlines at different flow rates for scheme 1. It can be seen from the pressure distribution that there is clearly a positive pressure gradient at the reflux hole; the pressure distributions on two sides of the reflux hole vary according to different rules. At a low flow rate ( $0.4Q_d$ ), the pressure on the separation chamber side is higher than on the other side of the reflux hole, so the fluid is forced to flow from the separation chamber to the volute through the reflux hole. This is because, at a low flow rate the pressure increases uniformly from the tongue to the outlet exit along the flow path. However, the pressure in the separation chamber is almost equal to the pressure at the volute outlet. The pressure at the separation chamber side of the reflux hole is

higher, which forces the fluid to flow back to the volute. The distribution state under design conditions ( $1.0Q_d$ ) is similar to the low-flow conditions and the pressure at the separation chamber side of the reflux hole is also higher. Under high-flow conditions ( $1.4Q_d$ ), the pressure distribution at the reflux hole is opposite to that at low flow rates and the pressure on the side of the volute is higher than on the separation chamber side, because the pressure decreases along the flow path for large flows. Hence, the pressure at the volute side of the reflux hole is higher, forcing the fluid to flow into the separation chamber.

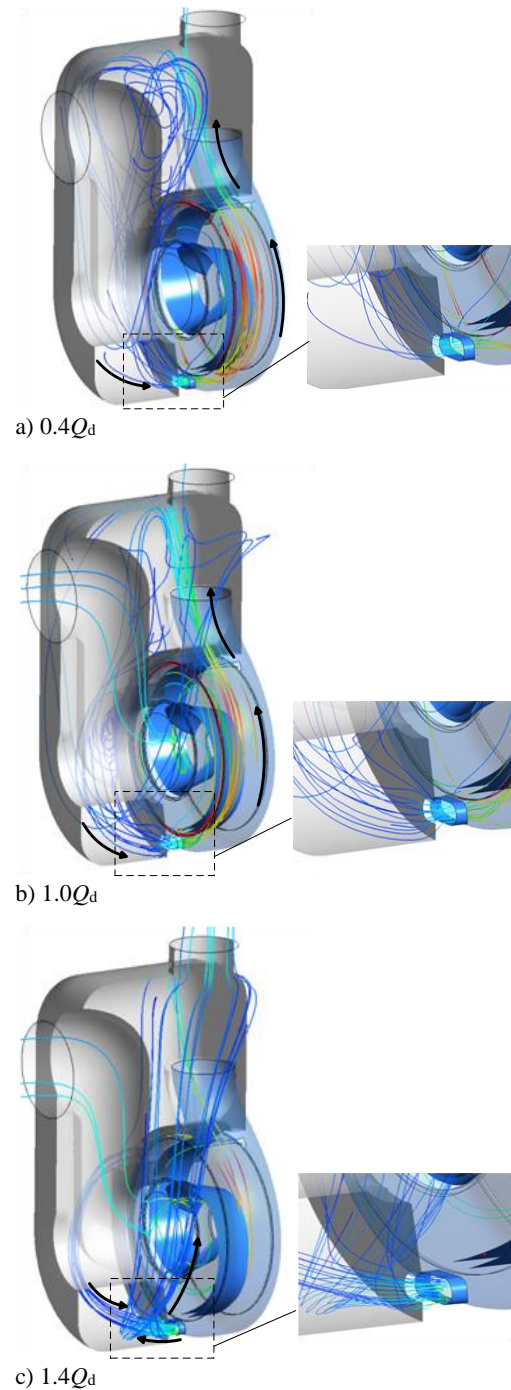


**Fig. 7. 3D streamlines under different working conditions.**

At low flow rates, it can be clearly seen that the fluid in the separation chamber flows smoothly into the volute casing through the reflux hole. There is an obvious positive pressure gradient on both sides of the reflux hole, which drives the flow smoothly into the volute from the bottom of the separation chamber. At the designed flow rate, streamlines at the bottom of the reflux hole are denser, demonstrating that the fluid cannot flow into the volute. This causes the flow in the separation chamber to form a vortex. At the same time, the pressure at the bottom of the reflux hole is relatively high. At large flow rates, the vortex in the chamber appears near the reflux hole, the fluid flowing into the reflux hole produces a vortex and reverse flow and the flow here is quite complicated. At the same time, a small amount of the fluid flows into the reflux hole from the volute and impacts on the fluid from the separation chamber. Simultaneously, the higher pressure in the volute forces the fluid into the separation chamber and forms a chaotic flow.

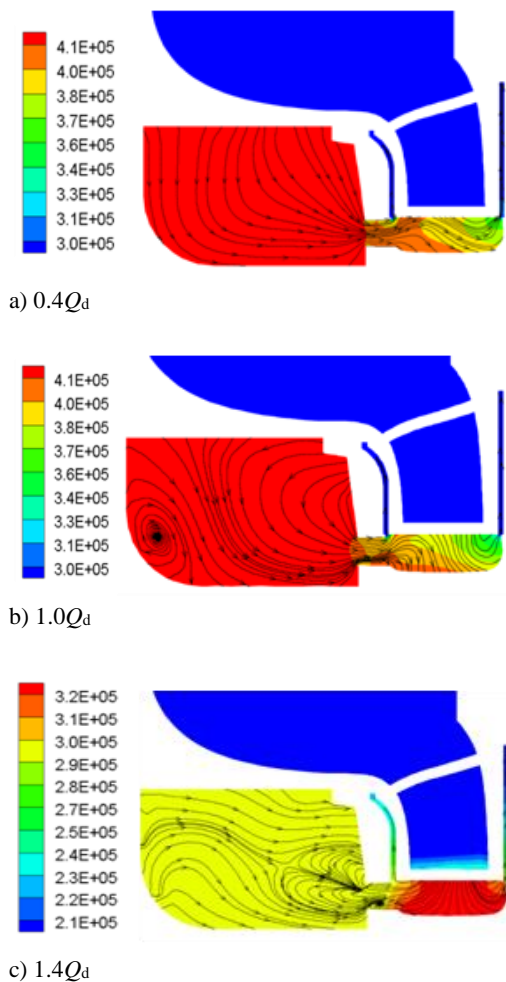


**Fig. 8. Static pressure distribution and streamlines under different working conditions.**

#### 4. DIFFERENTIAL PRESSURE AND REFLUX QUANTITY

Figure 9 shows the differential pressure between

two sides of the reflux hole for scheme 1, scheme 2 and scheme 3. As shown in Fig. 9, considering that the pressure in the separation chamber minus that in the volute is positive, it is found that the differential pressure has a descending trend with increasing flow rate. At low flow rates the pressure in the separation chamber is larger than that in the volute, and at large flow rates the pressure in the separation chamber is smaller than that in volute. It can be concluded that there is a critical state of zero differential pressure around the best-efficiency point of the pump. It can be seen from Fig. 9 that the zero differential pressure point of the pump will rise for large flow conditions with a decrease in reflux hole area.

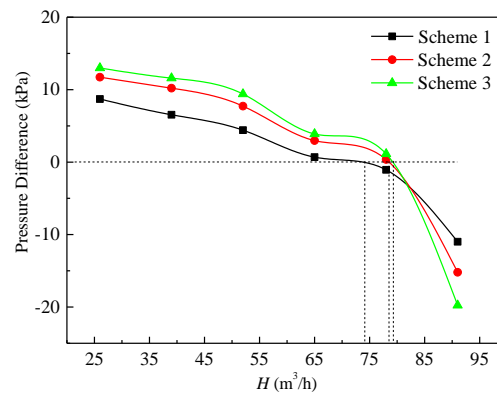
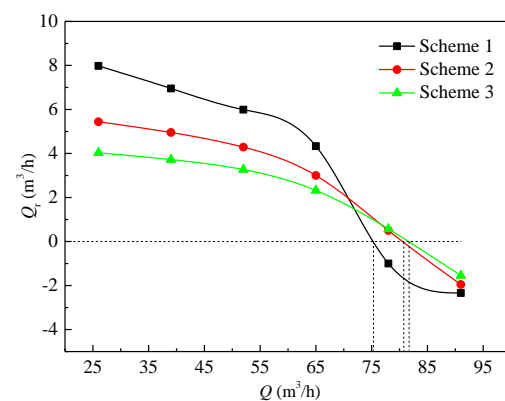


**Fig. 9. Differential pressure with the change of flow rate.**

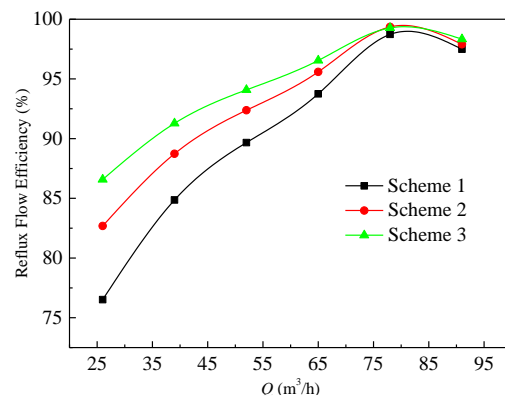
Figure 10 shows the reflux quantity and volumetric efficiency through the reflux hole for scheme 1, scheme 2 and scheme 3. As shown in Fig. 10, it is found that there is a critical state of zero reflux, which is almost consistent with the zero differential pressure point. Near the critical state point, the volumetric efficiency is largest. Considering that the reflux quantity is positive for fluid flowing into the volute, when working conditions are lower than the best-efficiency point, the reflux quantity reduces with increasing flow rate and when working conditions are higher than the best-efficiency point, the absolute value of the reflux quantity increases with increasing flow rate. Comparing the three schemes, along with the decrease in reflux hole area, the reflux quantity gradually reduces at the non-best efficiency points and the absolute value of the reflux quantity also gradually reduces at the large flow-rate points. It is also shown that the best-efficiency point of the pump shifts to a larger flow condition with a decrease in the reflux hole area. The change in the reflux quantity directly leads to changes in the leakage loss and finally, reflects the change in head and efficiency. If the reflux hole area is too large, it will result in serious leakage loss under low-flow conditions and the effect on pump energy performance will be very disadvantageous.

Theoretically, at the designed flow rate the best reflux hole area can result in zero pressure gradient between the two sides of the reflux hole. The pump efficiency can reach the optimum because almost no circulation flow loss is caused by the reflux hole (Chen, 1998; 1990). However, the critical state is

very difficult to achieve in a practical engineering application. Hence, we can only reduce the value range to be as small as possible, design a reasonable reflux hole area and minimize leakage loss while meeting the requirements of the self-priming performance. It can be seen in Fig. 10 that the reflux quantity of scheme 1 is obviously greater than for the other two schemes, especially at low flow rates. This indicates that the reflux hole area of scheme 1 is too large. Combining Fig. 7 and Fig. 10, it can be seen that the flow rates at the best-efficiency points of scheme 2 and scheme 3 are larger than  $1.4Q_d$ . The flow rate is too large, so that the pump cannot operate at a high efficiency under the designed conditions, which indicates that the reflux hole areas of scheme 2 and scheme 3 are too small.



a) Volumetric quantity



b) Volumetric efficiency

**Fig. 10. Reflux flow with the change in flow rate.**

### 5. TRANSIENT FLOW INSIDE VOLUTE AT THE REFLUX HOLE

Figure 11 shows the vorticity distribution and streamlines at different times in the cross section at the bottom of the volute when there is no reflux hole (Scheme 4,  $1.0Q_d$ ).  $T$  represents the passing period of the blade, As shown in Fig. 4, the blade is slightly in front of the reflux hole at  $T/4$ , and slightly after the reflux hole at  $2T/4$ . As shown in Fig. 11, each moment of the vorticity distribution was roughly the same. Nevertheless, because the blade has just swept over the reflux hole there are

flow disorders which result in an increase of vorticity in the middle part of the cross section at  $2T/4$ . The vorticity inside the cavities before and after the impeller is also relatively large; this is because the fluid in the cavities is limited, leading to a large number of vortices originating from the rotating impeller cover plate. There is an obvious transient characteristic about the streamline distribution in Fig. 11. The reverse secondary flow vortices on both sides of the volute are symmetrical in position but their sizes are different, which leads to a periodic change in the trend with first an increase and then a decrease to the point of disappearance.

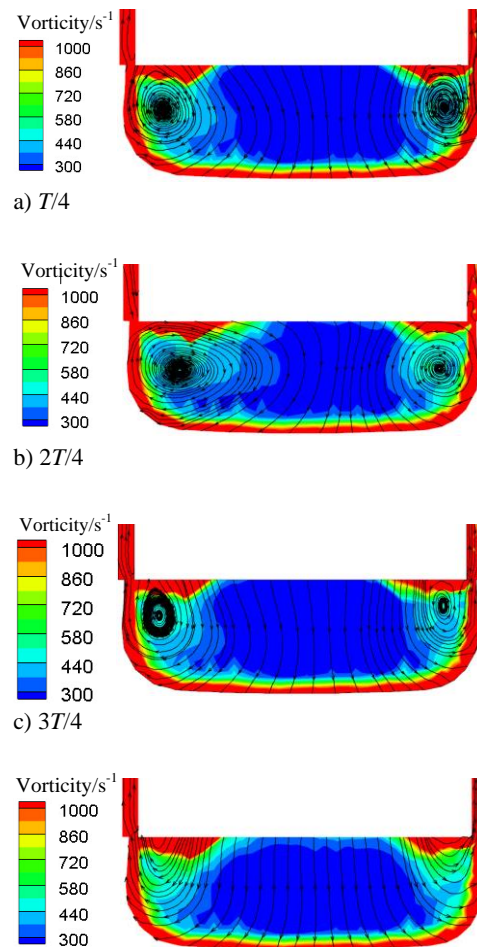


**Fig. 11. Cross-section at volute bottom of X axis direction.**

Figure 12 shows the vorticity distribution and streamlines in the volute cross section at the reflux hole, together with the time history (scheme 1,  $1.0Q_d$ ). As shown in Fig. 12, the vorticity was significantly larger in the area of the reflux hole exit than in other areas, reducing gradually within the volute. This is because the collision of the fluid flowing through the reflux hole into the volute and the fluid which is rotating at high speed in the volute, results in flow turbulence and large curl in the flow direction. The streamline distribution in

Fig. 12 shows that the backflow via the reflux hole disperses the original secondary flow vortex on the volute side: most of the reflux fluid flows into the volute and changes direction, while a small amount flows into the fore and back cavities, causing the asymmetric vortex structure in the cross section. On the other side of the volute, there was an obvious secondary flow vortex at  $T/4$ , when at  $2T/4$ , the vortex had developed large enough size, due to the fact that the high-speed rotating blade had just swept over the reflux hole. Subsequently, it decreased to some extent at  $3T/4$  and almost disappeared at  $T$ .

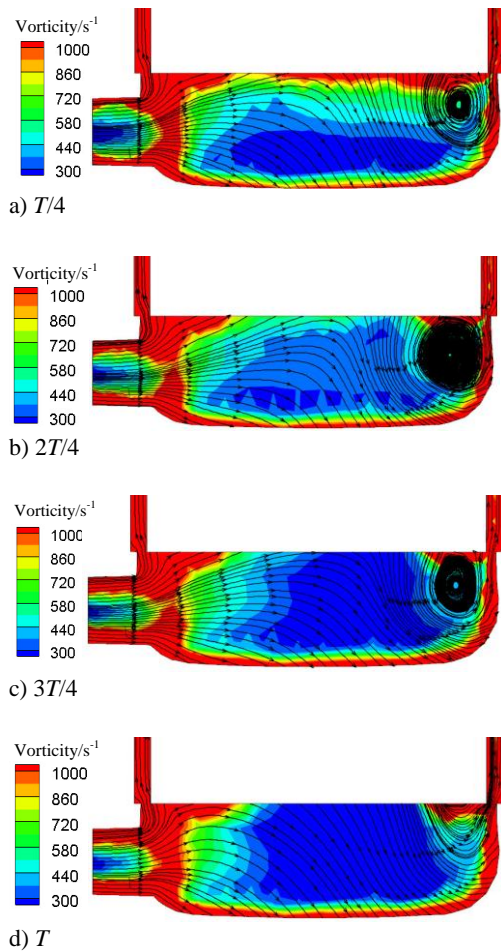


**Fig. 12. The volute cross-section at reflux hole of the X axis direction.**

Through the contrast analysis of flow characteristics at the volute reflux hole in Fig. 11 and Fig. 12, it can be concluded that, when the self-priming centrifugal pump operates normally, the existence of the reflux hole makes the volute produce an obviously asymmetric flow structure inside, and this will show a periodic change following the blade. In combination with the RSI (rotor-stator interaction) between the impeller and the volute, this makes the unsteady flow more complicated inside the volute, which will cause severe liquid vibration. Thus, it will exacerbate the pressure fluctuations in the volute and increase the hydraulic loss.

## 6. EFFECT OF REFLUX HOLE ON THE PRESSURE FLUCTUATION AND ENERGY PERFORMANCE

### 6.1 Pressure Fluctuation Characteristic

The monitored pressure fluctuations tend to be stable after five impeller rotation cycles. The monitoring data recorded between six and nine cycles were selected for statistical analysis, and the pressure fluctuation time-domain diagrams were obtained. Then the pressure fluctuation frequency-domain diagrams were subjected to a fast Fourier transform (FFT). In related centrifugal pump research (Lang, 2016; Wang, 2010), the dimensionless pressure fluctuation coefficient was introduced, in order to express the fluctuation characteristics more intuitively:

$$C_p = \frac{\Delta p}{0.5\rho u_2^2} \quad (3)$$

where  $\Delta p$  is the difference between the instantaneous static pressure and the mean pressure,  $\rho$  is the fluid density and  $u_2$  is the circumferential velocity at the impeller outlet.

The time domains of the pressure fluctuation at the monitoring points for the investigated pump at the design flow rate (scheme 1) are shown in Fig. 13. It can be seen that the trends of the pressure fluctuations at all the monitoring points are almost consistent, showing obvious periodicity. Within one rotating cycle, there are two peaks and two troughs in the time-domain diagram, because the impeller consists of two blades. Comparing the pressure fluctuation time domains of all the points, the peak value of  $P_2$  is the most dramatic, and the values of the other points further away from the tongue are lower.

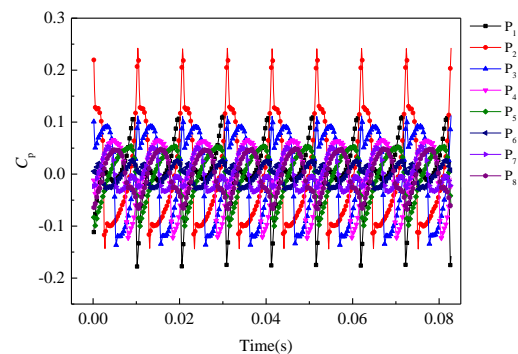


**Fig. 13. Pressure fluctuation time-domain diagram at monitoring points.**

Figure 14 shows the frequency domains of the pressure fluctuations at the monitoring points, which were obtained by the FFT at the design flow rate (scheme 1). According to Fig. 14, the pressure fluctuation frequencies are mainly concentrated in the low-frequency region. The dominant frequency is the blade passing frequency (96.67 Hz) or multiples of the blade passing frequency. It can be concluded that the pressure fluctuation is mainly induced by the RSI between the impeller and the

volute. The amplitude of the pressure fluctuations in the high-frequency region is relatively weak, as can be seen from the images of the frequency domains. This indicates that the amplitude at the monitoring points is gradually reduced in the impeller rotation direction while leaving the frequency component unchanged and the pulse energy gradually vanishes in the process of delivery. It can also be seen that the pulse amplitude at monitoring points P<sub>2</sub>-P<sub>5</sub> between the tongue and the reflux hole are considerably larger. The influence of the reflux hole area on the pressure fluctuation intensity at P<sub>2</sub>-P<sub>5</sub> will be selectively analysed below.

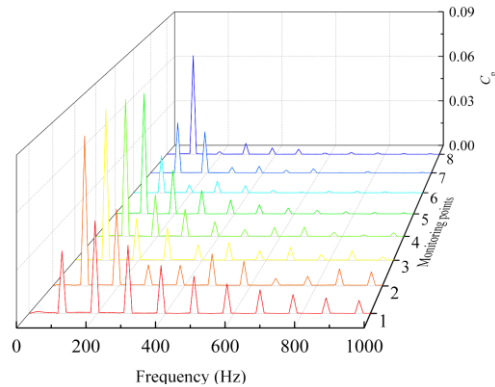
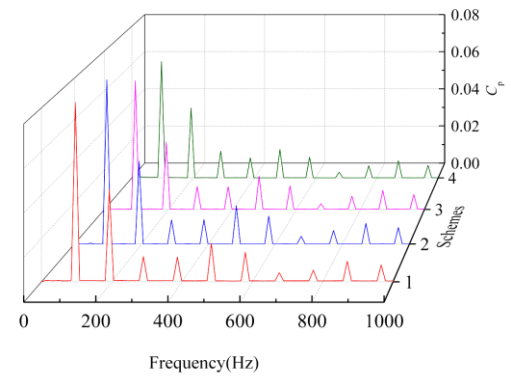


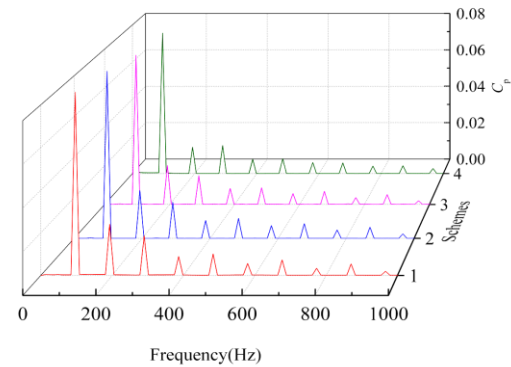
**Fig. 14. Pressure fluctuation frequency-domain diagram at monitoring points.**

The maximum amplitudes of pressure fluctuations from the different schemes were analysed. It was found that the pressure fluctuation at P<sub>1</sub> for the different schemes showed no obviously regular change, because it is mainly affected by the rotor-stator interaction. The pressure fluctuation intensities at monitoring points P<sub>2</sub>-P<sub>5</sub> upstream of the reflux hole were generally larger than those without the reflux hole and decreased as the reflux hole area decreased. This is caused by the reflux flow and the rotor-stator interaction working together. Strong hydraulic vibration is produced by impact with the tongue, and part of the vibrating fluid along the impeller rotation direction rapidly shoots into the volute through the gap between the impeller and the volute tongue. Then, impact at the volute wall causes a strong vortex, leading to intense pressure fluctuations. At the same time, the backflow through the reflux hole causes the upstream flow to be blocked, so the flow becomes more turbulent, thereby causing the intense pressure fluctuation phenomenon. With an increase of reflux hole area, the pressure fluctuation will be even more intense, because of the increase in backflow. However, the pressure fluctuations at monitoring points P<sub>6</sub>-P<sub>8</sub> downstream of the reflux hole generally increased with a decrease in reflux hole area, because the reflux liquid causes the velocity of the downstream liquid to increase, and the rapid flow eases the pressure fluctuation to some extent. The pressure fluctuation frequency domains at P<sub>2</sub>-P<sub>5</sub> for the different schemes under design conditions are shown in Fig. 15, which intuitively shows that the pressure fluctuation intensity decreases with a decrease in reflux hole area and is at a minimum for

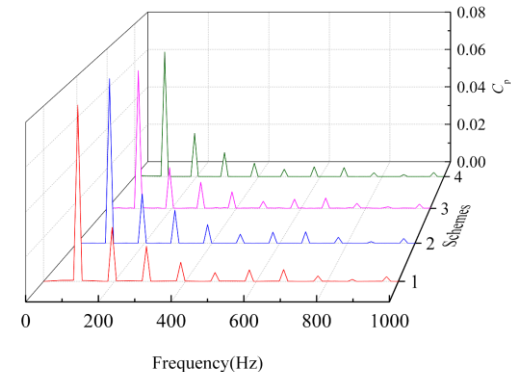
scheme 4 (without the reflux hole).



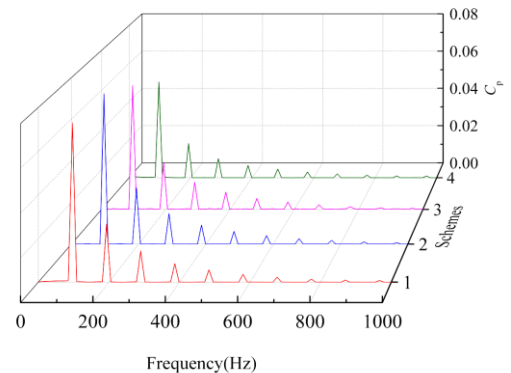
a) P<sub>2</sub>



b) P<sub>3</sub>



c) P<sub>4</sub>



d) P<sub>5</sub>

**Fig. 15. Frequency-domain diagram at P<sub>2</sub>-P<sub>5</sub> in different schemes.**

## 6.2 Analysis of Energy Performance

The calculation results for the energy performance are shown in Fig. 16. With decreasing reflux hole area, the efficiency and head of each working condition are improved to different degrees. The efficiency and head without the reflux hole are obviously higher than those with reflux holes, though the head gap is not obvious for the large flow. This is because less liquid flows through the reflux hole at large flow rates, with little leakage loss, so the head difference is not large. However, due to the complexity of the flow state at the reflux hole, a large number of vortices are produced, leading to significant hydraulic loss, so there is a significant difference in the efficiency at large flows.

The volume loss is caused by the leakage loss of the reflux hole, which is one of the most important factors leading to low efficiency in the self-priming pump. The reflux hole area has a close relationship with the change of head and the efficiency; therefore, the key point in the self-priming pump design is to reduce the value range of the reflux hole area, making it as small as possible. The leakage loss caused by the reflux hole should be reduced as far as possible while satisfying the self-priming property, to ensure the stable and efficient running of the self-priming centrifugal pump. Based on the above analysis, the optimum reflux hole area for the investigated pump should be 330-400 mm<sup>2</sup>.

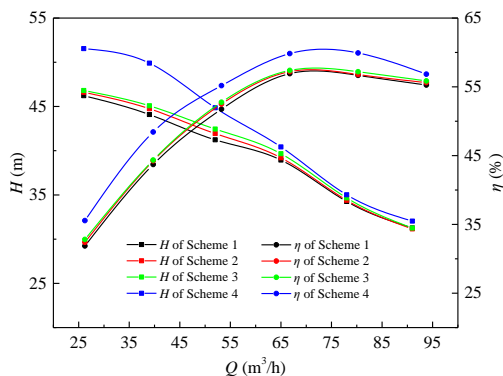


Fig. 16. The energy performance curves of different scheme.

## 7. CONCLUSIONS

Via the unsteady flow numerical simulations, the effects of the reflux hole on the transient flow characteristics and energy performance were analyzed. The results can be summarized as follows:

1) At the low flow rate, there is back flow from the gas-liquid separation chamber to the volute, which then flows into the separation chamber again. Thereby, the volume loss is increased by an annular flow. At the designed flow rate, annular flow also occurred in the separation chamber, but it was relatively stable. However, the pressure in the volute casing increases at the large flow rate, so it can hold back the reflux flow due to the large

pressure gradient.

2) At the low-flow-rate points, the pressure in the separation chamber is larger than that in the volute, so the fluid in the separation chamber is forced to flow into the volute through the reflux hole, and the reflux quantity reduces with increasing flow rate. At larger flow-rate points, the pressure at the separation chamber side is higher, which forces the fluid to flow back to the volute, and the absolute value of the reflux quantity increases with increasing flow rate. Theoretically, there is a critical state where both the differential pressure and the reflux quantity are zero. The efficiency and head will be improved with a decrease in reflux hole area.

3) The vorticity at the exit of the reflux hole is significant, and there are unsymmetrical vortex flow structures that change periodically over time in the cross section. This special unsymmetrical flow structure induced by the reflux flow not only exacerbates the pressure fluctuation intensity but also makes the unsteady flow more complicated inside the volute. Thus, it leads to serious hydraulic loss.

4) The dominant frequency of the pressure fluctuations belongs to the low-frequency regime, which is the blade passing frequency (96.67Hz) or multiples of this frequency. It can be concluded that the pressure fluctuation is mainly induced by the RSI between the impeller and the volute. The pressure fluctuation intensities at monitoring points P<sub>2</sub>-P<sub>5</sub> upstream of the reflux hole are generally larger than those without the reflux hole and decrease with decreasing reflux hole area. This is caused by the reflux flow and the RSI, working together.

## ACKNOWLEDGMENTS

This work was supported by the National Natural Science Foundation of China (Grant Nos. 51709234, 51779226), the Zhejiang Provincial Natural Science Foundation of China (Grant No. LQ17E090005), and the Open Research Subject of Key Laboratory of Fluid and Power Machinery (Xihua University), Ministry of Education (Grant No. szjj2016-076).

## REFERENCES

- Chen, M. Q. (1990). The research and design in reflux hole of self-priming centrifugal pump. *Journal of Fluid Engineering* 1990(3), 10-15.
- Chen, M. Q. and W. D. WU (1998). The study on the influence of reflux hole of the self-priming centrifugal pump self-priming performance. *Water Pump Technology* 1998(1), 26-30.
- Derakhshan, S., B. Mohammadi and A. Nourbakhsh (2008). Incomplete sensitivities for 3D radial turbomachinery blade optimization. *Computers & Fluids* 37(10), 1354-1363.
- González, J. and C. Santolaria (2006). Unsteady

- flow structure and global variables in a centrifugal pump. *Journal of Fluids Engineering* 128(5), 937-946.
- González, J., J. Fernandez and E. Blanco (2002). Numerical simulation of the dynamic effects due to impeller-volute interaction in a centrifugal pump. *Journal of Fluids Engineering*, 124(2), 348-355.
- Guan, X. F. (2011). Modern pump theory and design. *China Aerospace Press*, Beijing, China, 424-430.
- Hermann, L. (1949). Self-priming centrifugal pump: U.S., Patent No. 2461925.
- Huang, S., X. Su and J. Guo (2014). Unsteady numerical simulation for gas-liquid two-phase flow in self-priming process of centrifugal pump. *Energy Conversion and Management* 85 (9):694-700.
- Hubbard, B. (2000). Self-priming pump characteristics of flexible impeller pumps. *World Pumps* 2000(405), 19-21.
- ISO 9906:2012, Rotodynamic pumps - Hydraulic performance acceptance tests - Grades 1 and 2. *International Standardization Organization*, Geneva.
- Kanute, J. (2004). Self-priming centrifugal pumps a primer. *World Pumps* (456), 30-32.
- Lang, T., W. D. Shi and K. Q. Chen (2016). Pressure fluctuation characteristics in centrifugal pump volute induced by super-thick blades. In *Energy and Mechanical Engineering: Proceedings of 2015 International Conference on Energy and Mechanical Engineering*, Wuhan, China, 879-887.
- Li, H., B. Jiang and T. Q. Lu (2015). The visualization test of gas-liquid two phase flow in self-priming pump process. *Transactions of the Chinese Society for Agricultural Machinery* 46(8), 59-65.
- Li, H., D. Xu and Q. Tu (2013). Numerical simulation on gas-liquid two-phase flow of self-priming pump during starting period. *Transactions of the Chinese Society of Agricultural Engineering* 29(3), 77-83.
- Li, H., Z. Shen and J. Liu (2010). Influence of pressure fluctuation on reflux valve in a self-priming pump with outer recirculation. In *ASME 2010 3rd Joint US-European Fluids Engineering Summer Meeting collocated with 8th International Conference on Nanochannels, Microchannels, and Minichannels*. New York, USA, 523-530.
- Li, T. B. (1982). Reflux hole on the self-priming performance and the influence of elastic valve. *Water Pump Technology* 4, 23-25.
- Liu, J. R. and Q.Q. Su (2009). The numerical simulation of gas and liquid two phase-flow in self-priming pump. *Transactions of the Chinese Society for Agricultural Machinery* 40(9), 73-76.
- Lv, Z. J., C. Y. Lan and F. J. Wang (2005). The Present status and development of self-priming pump. *Journal of Drainage and Irrigation Machinery Engineering* 23(3), 1-5.
- Sha, Y., S. Q. Yuan and Y. F. Han (1999). The experimental study on improving the performance of outer recirculation self-priming pump. *Water Pump Technology* 1999(6), 20-22.
- Shepard, J. (2003). Self-priming pumps: an overview. *World Pumps* 2003(444), 21-25.
- Shi, W., C. Wang and W. Wang (2014). Numerical calculation on cavitation pressure pulsation in centrifugal pump. *Advances in Mechanical Engineering* 2014(6), 1-8.
- Tan, L., B. Zhu and Y. Wang (2015). Numerical study on characteristics of unsteady flow in a centrifugal pump volute at partial load condition. *Engineering Computation* 32(6), 1549-1566.
- Wang, C., Z. Wu and Y. Si (2009). Gas-liquid two-phase flow numerical simulation of a vortex flow self-priming pump. *Drainage & Irrigation Machinery* 27(3):163-167.
- Wang, K., Z. Zhang and L. Jiang (2017). Effects of impeller trim on performance of two-stage self-priming centrifugal pump. *Advances in Mechanical Engineering* 9(2), 1-11.
- Wang, Y. and C. Dai (2010). Analysis on pressure fluctuation of unsteady flow in a centrifugal pump. *Transaction of the Chinese Society for Agricultural Machinery* 41(3), 91-95.
- Wu, D., S. Yang and B. Xu (2014). Investigation of CFD calculation method of a centrifugal pump with unshrouded impeller. *Chinese Journal of Mechanical Engineering* 27(2), 376-384.
- Yi, Q. (1991). Outer recirculation self-priming centrifugal pump self-priming performance influence factors analysis and fault rule out. *Journal of Drainage and Irrigation Machinery Engineering* 9(1), 1-7.
- Yuan, Z., J. Jiliang, and Z. Liyuan, (2015). Single Stage Horizontal Self-Priming Pump System Assembly and Kinematics Simulation. *Advanced Communication and Networking, 2015 Seventh International Conference on*. *IEEE*. Kota Kinabalu, Malaysia. 36-39.